Internet of Things 26 (2024) 101236

Contents lists available at ScienceDirect

Internet of Things

journal homepage: www.elsevier.com/locate/iot

Research article

Indoor position estimation using angle of arrival measurements: An efficient multi-anchor approach with outlier rejection ☆

Guillem Boquet [a,*], Aleix Boquet-Pujadas [b], Ivan Pisa [a], Anand Dabak [c], Xavier Vilajosana [a], Borja Martinez [a]

[a] Wireless Networks Group, Universitat Oberta de Catalunya, Barcelona, Spain
[b] Biomedical Imaging Group, École polytechnique fédérale de Lausanne, Lausanne, Switzerland
[c] Texas Instruments Inc., Dallas, TX, USA

ARTICLE INFO

Keywords:
Internet of Things
Localization
Angle of arrival
Position estimation
Outlier filtering
Anchor selection

ABSTRACT

This paper addresses the inherent nonlinear problem in indoor position estimation utilizing Angle of Arrival (AoA) measurements. We investigate the influence of deployment geometry on system performance through both analytical methods and Monte-Carlo simulations, shedding light on the limitations of single and multi-anchor setups and underscoring the imperative for advanced multi-anchor localization methods. In response to this problem, we propose a multi-anchor solution with outlier rejection that efficiently considers the nonlinearity of the model. For each anchor, our approach approximates the probability distribution of the node position by leveraging a geometrically-derived unscented transformation of AoA estimates. The approximations are then integrated into a majority voting scheme, effectively eliminating outliers induced by multipath or other adverse effects. To derive the final enhanced position estimate, Bayesian inference is applied to fuse the selected information. Finally, the efficacy of the solution is validated conducting a comparative analysis against commonly used approaches in a real-world Bluetooth indoor localization system. The results obtained solely from high-level angular measurements underscore the practicality, robustness and high accuracy of the proposal.

1. Introduction

The growing capabilities and performance improvements in cyber–physical systems are reshaping industries and social environments. They empower individuals to address increasingly complex challenges through automation and the exploitation of data. These advancements result in services that elevate the quality of both work and everyday life [1]. A pivotal element in this digital transformation is the integration of indoor localization with the Internet of Things (IoT) [2]. Much like how Global Navigation Satellite Systems (GNSS) revolutionized logistics and transportation, indoor localization is poised to bring about significant changes in various applications, including robotics, storage management, security, healthcare and more [3].

The current IoT has evolved significantly, tackling various technologies to create a diverse framework with multiple methods for locating indoor assets. These techniques comprehend a wide spectrum, from the analysis of camera images to smart radio-frequency identification [4]. In wireless communication, measurements of distinct parameters such as Channel Status Information (CSI), Received Signal Strength Indicator (RSSI), Angle of Arrival (AoA), Angle of Departure (AoD), Time of Arrival (ToA) or Time

☆ This work is co-funded by the Spanish Ministry of Science, Innovation and Universities (RF-VOLUTION project, PID2021-122247OB-I00); the Catalan Department of Research and Universities (SGR 00174 2021); and the European Union's Horizon 2020 (VEDLIoT project, No 957197). Prof. Xavier Vilajosana is supported by ICREA Academia Grant.

* Correspondence to: Universitat Oberta de Catalunya, Rambla del Poblenou 154-156, 08018 Barcelona, Spain.
E-mail address: gboquet@uoc.edu (G. Boquet).

https://doi.org/10.1016/j.iot.2024.101236
Received 30 August 2023; Received in revised form 24 May 2024; Accepted 25 May 2024
Available online 27 May 2024

Difference of Arrival (TDoA) can be processed to derive an estimated position of the asset [3,4]. Notably, the Bluetooth Special Interest Group (SIG) introduced direction-finding capabilities in version 5.1 of the Bluetooth Core Specification. This update precisely defines the architecture for identifying the AoA and AoD of a transmitted Bluetooth Low Energy (BLE) signal [5,6]. It is important to note, however, that the specification does not prescribe any specific angle or position estimation algorithms. Nevertheless, this advancement has accelerated the adoption of this technology and has led to the proliferation of closed localization solutions in the IoT market [7]. Within this context, this article focuses on IoT indoor localization using AoA measurements from cost-effective solutions tailored for affordable setups, such as BLE-based ones. Our primary emphasis is on scalable methods designed for low-power and low-cost devices capable of real-time operation, enabling ubiquitous localization for the IoT.

AoA-based localization systems consist of a collection of anchored nodes strategically positioned to localize mobile nodes within a specific reference frame. The azimuth angle and elevation angle define the AoAs [7], effectively describing the vector connecting the mobile node and the anchor node. These angles serve as crucial parameters for determining the mobile node's location. In general, the localization process entails deducing, from the perspective of the anchor node, the direction from which the signal emitted by the mobile node originates. To achieve a precise directional estimate, it is imperative to account for various signal effects, including multipath components, polarization, spread delays, jitter and noise [8]. Subsequently, the angle information is translated into an absolute Cartesian position estimate, the focus of this article.

This article delves into the limitations associated with both single and multi-anchor localization setups utilizing AoA measurements. The first contribution lies in evaluating the most effective strategy for combining measurements obtained in multi-anchor deployments. Through analytical derivations and Monte Carlo simulations, this study provides valuable insights into the influence of deployment geometry and the nonlinear conversion of angles into position coordinates on system performance. Our findings unequivocally highlight the relationship between expected accuracy and the node's positioning relative to the deployment geometry. It is crucial to note that the mere combination of data from multiple anchors does not necessarily lead to more precise estimates.

Addressing this challenge constitutes the second goal and the key contribution of this work. We propose a probabilistic solution designed to efficiently utilize multiple observations from distinct anchor locations, all originating from the same signal source. The introduced algorithm significantly enhances position estimation accuracy by identifying and discarding outliers through a majority voting scheme. Furthermore, it iteratively updates the probability distribution of the node's location based on information from selected anchors, employing Bayesian inference. This iterative probability update culminates in a final position estimate that integrates the chosen information.

The algorithm offers several advantages, including efficient handling of nonlinearity, practicality through an approximation that avoids expensive non-convex optimization processes, and robustness due to outlier rejection. Demonstrating its scalability for IoT applications, the algorithm seamlessly incorporates additional angle or position information. Simultaneously, it achieves sub-meter accuracy in a real-world BLE localization system, as verified through testing. Importantly, our method relies solely on high-level position or angular measurements, making it compatible with a broad array of IoT location technologies beyond BLE. This adaptability is particularly advantageous given that vendors often do not publicly disclose low-level metrics in numerous applications and services.

The structure of this article is organized as follows: Section 2 provides background information and discusses related work. Section 3 outlines the definition of the localization system. Section 4 explores the nonlinear problem in AoA-based localization systems. Section 5 introduces a dedicated filter designed to address the problem. Section 6 details the experimental evaluation conducted to assess the proposed method. Finally, Section 7 concludes the article.

2. Background and related work

Indoor localization techniques in the IoT domain utilize angle estimates, employing methods ranging from simple lateration and angulation to complex collaborative approaches involving various measurements (such as RSSI, ToA and AoA) and diverse radio technologies like WiFi, BLE and Ultra-wideband (UWB). For a comprehensive review of indoor localization methods, readers are encouraged to explore surveys conducted by Zafari et al. [3] and Guo et al. [9], which focus on fusion-based approaches.

2.1. Brief introduction to signal direction estimation

Estimation of signal direction constitutes the initial phase of the localization process. This direction can be estimated by equipping each anchor with a directional antenna or antenna array. In the case of anchors equipped with a Radio Frequency (RF) antenna array, whether linear, rectangular, or circular, the incoming signal will arrive at each antenna with slight time and phase delays, resulting in variations from the original signal. Since the spacing between antennas is designed and known, signal direction can be estimated using processing techniques that aim to extract embedded angle information. A practical example of this is found in the optional Constant Tone Extension (CTE) of a Bluetooth packet, which is explicitly designed for this purpose in the standard [7]. The CTE itself does not convey information but facilitates an RF switch to sequentially sample the same signal across different antennas in time, reducing both space and hardware costs. Initially, anchors sample the In-phase (I) and Quadrature (Q) components of the received signal. Subsequently, the IQ samples are further processed to derive angle estimates. This process takes into account various factors, including sensor noise, hardware imperfections, antenna switching, limited observations and signal propagation distortions such as attenuation and multipath effects.

Processing algorithms can be categorized into four groups based on specific techniques: array antenna beamforming, signal and noise subspace decomposition, sparse space representation and parametric search using Maximum Likelihood Estimators (MLE). For

more detailed insights into these methods, readers are encouraged to consult Krim et al. [10], which offers a comprehensive overview in array signal processing. As examples, the Minimum Variance Distortionless Response (MVDR) and MUltiple Signal Classification (MUSIC) are well-established estimators in the first two categories, respectively. Nevertheless, despite advancements in antenna design and processing algorithms, angle estimate errors can still be significant due to the inherent randomness of the RF medium and its dynamic behavior in indoor environments.

2.2. Position estimation using angular measurements

The subsequent stage of the localization process involves position estimation utilizing the estimated AoAs, which is the primary focus of this article. This section provides a review of the state-of-the-art AoA-based position estimation in IoT.

2.2.1. Single-anchor

It is typically assumed that the node lies on a surface in most IoT applications, thereby eliminating the need to estimate its altitude, e.g., when tracking a shopping cart inside a supermarket. When the z coordinate of the node is predefined, the derivation of a position estimate requires only the signal direction estimate from a single anchor. The geometric solution for a single anchor involves finding the point of intersection between the line formed by the anchor's position and the direction of the received signal and the plane where the node is assumed to be located. This solution becomes non-unique only if the line is parallel to or falls within the plane, a scenario with a negligible probability when dealing with noisy measurements.

The non-linearity of this problem exert a substantial influence on position error. The position error significantly differs from the error in the initial angle estimation, thereby constraining the performance as elaborated in Section 4.

2.2.2. Multi-anchor

Deploying multiple anchors and combining their information aims to mitigate the limitations of a single anchor. For accurate position estimation in a three-dimensional (3D) space, angles from at least two anchors are essential, while only their azimuth angles suffice for a two-dimensional (2D) estimate. Real-world factors often necessitate the involvement of more than two anchors to enhance accuracy.

Employing multiple anchors introduces complexities leading to potential ambiguities in position estimation that can be resolved through heuristic methods and multiangulation techniques. One straightforward approach involves computing the centroid of individual estimations from each anchor using the sample-mean estimator, allowing for the combination of estimates from various technologies or methods. A more advanced solution entails the Least-Squares (LS) minimization of the sum of squared perpendicular distances from the unique solution point to the lines defined by the anchor positions and their received signal direction [11]. Alternatively, several other localization techniques tailored for Gaussian noise have been proposed, such as the direct grid search method, the pseudo-linear estimator and the Maximum Likelihood Estimation (MLE) [12–16]. However, these methods may not offer an optimal means to combine multiple observations, often necessary for improving accuracy in indoor environments with multipath interference [17]. Machine learning approaches that require offline training phases have been proposed, such as fingerprinting and K-Nearest Neighbor (KNN) [18]. Hybrid solutions that combine different measured parameters also exist. For instance, Ding et al. [19] developed a method based on error variance and measurement noise weighted LS, incorporating RSSI and AoA measurements, a low-energy and narrowband solution. Geng et al. [20] conducted experiments validating probabilistic joint localization with ToA and AoA measurements based on directional statistics, employing a dual-radio and wideband approach.

Directional statistics are frequently employed to account for the periodic nature of angles, mitigating the nonlinearity and singularity challenges associated with Cartesian-polar models [21]. The resulting optimizations typically yield non-convex problems, leading to scalability challenges, high computational costs and a lack of stability and optimization guarantees—critical considerations in the context of IoT, where practicality and reliability are paramount. Henninger et al. [22], propose an initialization routine and a gradient-based optimization procedure to mitigate these concerns. Instead, we circumvent the problem of non-convexity by introducing an approximation for the probability distribution of the node position in the Cartesian-polar model. This approximation is achieved through a geometrically-derived unscented transformation of AoA estimates.

2.2.3. Anchor selection

The mentioned solutions exhibit sensitivity to outliers [23,24]. To address this issue, anchor selection methods opt for selecting a subset of anchor information, which leads to improved position estimates.

The majority of anchor selection techniques commonly assume that the closest anchors offer the most reliable angular information. RSSI measurements are frequently deemed valuable since they theoretically correspond to distance through appropriate propagation models. However, it has been observed that RSSI measurements do not consistently correlate with actual distances in indoor environments [25]. Alternative selection techniques leverage channel characteristics or other metrics to quantify the uncertainty in angle estimates, thereby reflecting the reliability of anchor information. For example, Van der Vorst et al. [26] employ a variance-based sensitivity index to eliminate anchors, indicating how each input variable contributes to output uncertainty. Monfared et al. [27] identify and mitigate non-line-of-sight (NLOS) anchors by comparing variances in intermediate estimated positions against predefined thresholds. Yan et al. [28] combat outliers through an iterative non-convex sparse optimization method, assuming Gaussian noise with known covariance. Xiong et al. [29] employ a weighted linear LS estimator for line-of-sight (LOS) components and a data selection technique that discards error-prone NLOS components. In contrast, the approach proposed in Section 5 utilizes a majority voting scheme to eliminate anchors with conflicting approximated position error distributions. This methodology takes into consideration the nonlinearity inherent in the estimation problem and acknowledges the geometric influence on dilution of precision. The presented approach provides a novel solution to address the outlier challenge in indoor localization.

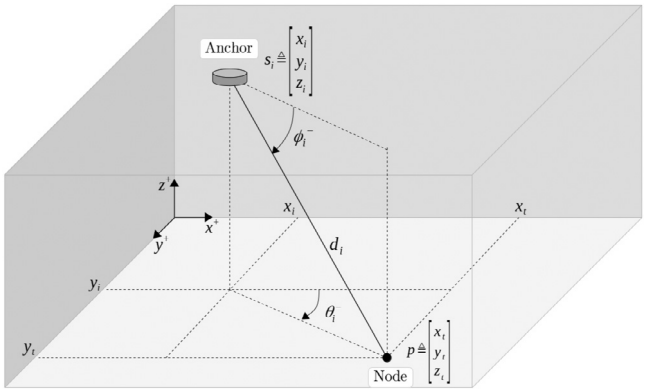

Fig. 1. Geometric depiction of the interaction between an anchored receiver antenna board and a mobile transmitter node in an AoA-based indoor localization system.

2.2.4. *Time filtering*

The presented approaches address static position estimation. It is crucial to note that not all use cases have the capability to exploit temporal correlations, especially in scenarios where samples may be spaced in time. This is particularly relevant in low-power use cases and various contexts within the IoT. However, in many practical scenarios, node positions exhibit temporal correlation, which can be leveraged for tracking and mitigating estimation inaccuracies in successive AoA measurements. The iterative process, commonly referred to as Bayesian filtering, can be realized through methods such as the particle filter and Kalman filter (KF), as discussed in [30]. For example, Gamarra et al. [31] propose a system that combines BLE AoA measurements and GNSS signals with a KF for indoor-outdoor asset tracking. While our article primarily focuses on static use cases, it is worth noting that our filtering algorithm can serve not only as a standalone solution but can also be synergistically combined with temporal filters to enhance tracking performance. Our algorithm can be effortlessly extended for tracking purposes by applying a KF to the localization outcomes at each time instance.

3. Definition of the localization system utilizing AoA measurements

This section defines the mathematical framework of the indoor localization system based on AoA measurements. The system illustrated in Fig. 1 utilizes a network of strategically positioned anchors, each equipped with a circular antenna array. These anchors detect incoming signals from a node in all directions, allowing for the determination of AoAs. The estimated AoAs are then employed to estimate the precise location of a node within the indoor space in static conditions.

Let $\mathbf{p} \triangleq \left[x_t, y_t, z_t\right]^\mathsf{T} \in \mathbb{R}^3$ denote the true position of the mobile node in a Cartesian coordinate system. Let $\mathcal{A}_n = \{\mathbf{s}_1, \dots, \mathbf{s}_n\}$ be the set of $n \geq 1$ anchor nodes, where the $\mathbf{s}_i \triangleq \left[x_i, y_i, z_i\right]^\mathsf{T} \in \mathbb{R}^3$ stand for their absolute fixed positions. Let $\boldsymbol{\theta}_n = \{\theta_1, \dots, \theta_n\}$ and $\boldsymbol{\phi}_n = \{\phi_1, \dots, \phi_n\}$ be the respective sets of true azimuths and elevations describing the AoAs of a wireless signal to each of the n anchors. These pairs of angles can be expressed geometrically in terms of the corresponding node positions as (see Fig. 1)

$$\theta_i = h_i^\theta(\mathbf{p}) = \arctan2\left(y_t - y_i,\, x_t - x_i\right), \tag{1}$$

$$\phi_i = h_i^\phi(\mathbf{p}) = \arcsin\left(\frac{z_t - z_i}{d_i}\right), \tag{2}$$

where $d_i \triangleq \|\mathbf{p} - \mathbf{s}_i\|_2 > 0$ is the Euclidean distance between the anchor and the mobile node. The choice $\left[\theta_i, \phi_i\right]^\mathsf{T} \in \Omega \triangleq [-\pi, \pi) \times \left[-\frac{\pi}{2}, 0\right]$ constrains ϕ to an indoor setting and avoids the indetermination of θ [32].

Let $\mathbf{z}_i \triangleq [\hat{\theta}_i, \hat{\phi}_i]^\mathsf{T} \in \Omega$ be the AoAs observed from the ith anchor, where $\hat{\theta}_i$ and $\hat{\phi}_i$ refer to the respective measurements of the azimuth and elevation angles. We write the observation model of the localization system in vector form as

$$\mathbf{z}_i = \mathbf{h}_i(\mathbf{p}) + \mathbf{w}_i \tag{3}$$

with $\mathbf{h}_i(\mathbf{p}) \triangleq [h_i^\theta(\mathbf{p}), h_i^\phi(\mathbf{p})]^\mathsf{T}$, and $\mathbf{w}_i \in \mathbb{R}^2$ a noise vector modeling the ensemble of unfavorable factors. In this setting, $\hat{\theta}_i$ and $\hat{\phi}_i$ can be regarded as two continuous random variables with joint probability density $p(\hat{\theta}_i, \hat{\phi}_i|\mathbf{p})$, and marginals $p(\hat{\theta}_i|\mathbf{p})$ and $p(\hat{\phi}_i|\mathbf{p})$ when conditioned to the true node position.

We now define the estimator $\hat{\mathbf{p}}$ of the node position as

$$\hat{\mathbf{p}} = f\left(\mathcal{Z}_n; \mathcal{A}_n\right), \tag{4}$$

where the function $f : \Omega^n \mapsto \mathbb{R}^3$ maps a set $\mathcal{Z}_n = \{\mathbf{z}_1, \dots, \mathbf{z}_n\}$ of AoAs measured from the fixed-anchor nodes $\mathcal{A}_n$ to an estimate of the position of the mobile node. The goal of a localization system is to derive a function f that maximizes the accuracy of $\hat{\mathbf{p}}$,

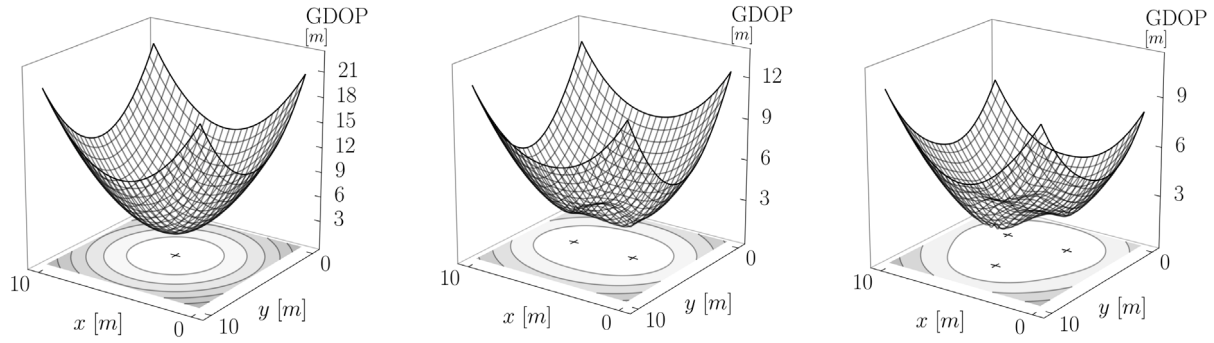

(a) Single anchor at $[5, 5, 3]^\mathsf{T}$ meters.

(b) Two anchors at $[7, 5, 3]^\mathsf{T}$ and $[3, 5, 3]^\mathsf{T}$ meters.

(c) Three anchors at $[7, 3, 3]^\mathsf{T}$, $[3, 3, 3]^\mathsf{T}$ and $[5, 7, 3]^\mathsf{T}$ meters.

Fig. 2. GDOP maps for different single and multi-anchor localization setups.

i.e., minimizes the distance between $\hat{\mathbf{p}}$ and $\mathbf{p}$. However, the nonlinear inversions in (1) and (2) –which are required to estimate $\mathbf{p}$ from the data $\mathcal{Z}_n$ via (3)– often amplify measurement noise and lead to estimates that are biased and that do not achieve minimum variance for small sample sizes [33]. Moreover, the computational complexity of these approaches hampers their application to real-time applications.

Finally, there are multiple ways to characterize the accuracy of a localization system. For example, the error covariance matrix describes the uncertainty of the resulting estimates as

$$\mathbf{P} \triangleq \mathbb{E}\left[(\hat{\mathbf{p}} - \mathbf{p})(\hat{\mathbf{p}} - \mathbf{p})^\mathsf{T}\right]. \tag{5}$$

The common system-level metrics and key performance indicators are the Cumulative Distribution Function (CDF) of the error, the Root Mean Squared Error (RMSE) and the Circular Error Probability (CEP):

$$\text{CDF}(\epsilon) \triangleq \mathbb{P}\left(\|\mathbf{p} - \hat{\mathbf{p}}\|_2 \leq \epsilon\right), \tag{6}$$

$$\text{RMSE} \triangleq \sqrt{\mathbb{E}\left[\|\mathbf{p} - \hat{\mathbf{p}}\|_2^2\right]}, \tag{7}$$

$$\text{CEP}_{95} \triangleq \{\rho \mid \mathbb{P}\left(\|\mathbf{p} - \hat{\mathbf{p}}\|_2 \leq \rho\right) = 0.95\}. \tag{8}$$

4. Navigating nonlinearity: Unveiling the need for advanced multi-anchor localization methods

The objective of this section is to expound how errors in the measured AoAs propagate through nonlinear equations (1) and (2) to influence the estimation of node positions. Ideally, minor deviations in the measured angles should result in negligible alterations in the output localization. However, this assumption does not hold true in AoA-based localization. The nonlinearity introduces several drawbacks, thereby emphasizing the necessity for advanced multi-anchor localization methods. In Section 5, we propose such a method as part of our primary contribution.

This section employs the critical concept of Geometric Dilution of Precision (GDOP) to illustrate and discuss how the theoretical interplay between the nonlinear model and the geometry of the setup impacts the estimation process in single and multi-anchor localization scenarios. The findings underscore the complexity of indoor systems and contribute valuable insights for designing robust localization solutions. GDOP is theoretically derived in Appendix A. It can be interpreted as the ratio of position RMSE to angle RMSE [34].

4.1. Limits of single-anchor localization

Fig. 2(a) presents the GDOP for 2D localization of a mobile node in a standard-sized room with a single anchor deployed. The function was computed using the provided expression in Appendix A.1. The minimum GDOP value of 3 m occurs when the mobile node is directly below the anchor at $z = 0$ m. The nonlinear nature of precision dilution is evident: As the hypothetical node moves away from the anchor, the sensitivity of position estimation to observed errors in angles increases significantly. Assuming an expected AoA estimation accuracy of 10° RMSE, position estimation errors rapidly become impractical at relatively short distances from the anchor for critical indoor use cases.

Given this limitation, one might anticipate that incorporating more anchors enhances localization accuracy by reducing, at least, the RMSE in the region under each anchor. This is straightforward for single-anchor selection methods, as the combination of

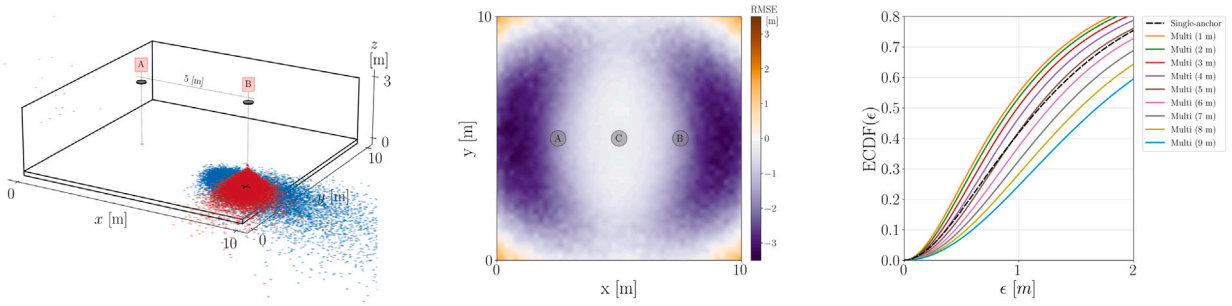

(a) Single point comparison. (b) Spatial comparison. (c) General comparison.

Fig. 3. Effect of GDOP on the naive fusion of multi-anchor estimates against the single-anchor solution in AWGN conditions.

n sufficiently separated anchors results in their respective minimum GDOP, when optimally selected. However, this task is more challenging for algorithms handling multiple anchors simultaneously because the GDOP is neither linear nor separable, see (28) in Appendix A. Analytically, the literature demonstrates that GDOP is a monotonically decreasing function of the number of anchors using when the MLE is used [35]. In this scenario, adding anchors reduces GDOP by increasing information in the Fisher Information Matrix (FIM), as seen in the summation of positive definite matrices in (26). Extending GDOP to a multi-anchor scenario, the findings from Figs. 2(b) and 2(c) reveal that precision dilution is reduced when the node is positioned within the convex hull area of the anchors. Each solid contour line projected at $z = 0$ m in Fig. 2 represents an integer multiple of the minimum GDOP. In comparison to the single-anchor figure, multi-anchor setups exhibit a decreased separation between lines. This is clearly observable in the center areas delimited by the first range of 3 to 6 m.

Unfortunately, the simplifying assumptions of GDOP that suit GNSS operating at large receiver-emitter distances do not align well with indoor deployments. Consider the high Signal-to-Noise Ratio (SNR) region, for example. The LS estimator often converges to the Cramér-Rao Bound (CRB) for large sample sets: It is precisely the MLE when the errors are Gaussian and the covariance is proportional to the identity matrix, that is, when the azimuth and elevation angles observed are uncorrelated and with equal variance and do not depend on the node position. The stated conditions, which are applicable to approximately equispaced anchors and nodes in GNSS, do not remain valid in indoor setups. In such environments, the noise variance is additionally proportional to varying distances between them, that is, the variance of angle errors strongly depends on node positions [36]. For instance, estimating azimuth angles for positions involving very vertical angles of elevation becomes more challenging. Additionally, an estimation bias exists in MLE due to the nonlinear nature of the localization problem, which is also geometry-dependent [37].

In conclusion, while the addition of anchors may improve system accuracy in ideal conditions due to a reduced GDOP, the challenge lies in handling multiple anchors simultaneously due to the nonlinearity and non-separability of the underlying equations. Also, there is an associated increase in operating costs when deploying multiple anchors, that is, a balance between achieving optimal accuracy and managing practical deployment costs.

4.2. Naive multi-anchor localization

In this section, we demonstrate that including information from additional anchors to naive estimators enhances the accuracy of single-anchor estimates only under specific conditions. Unfortunately, these conditions are not always met in indoor localization deployments.

Let us consider the problem of estimating the position $\mathbf{p}$ of a static node by naively combining, using the sample-mean estimator, position estimates from two independent anchors: anchor A and anchor B. The theoretical conclusion is that incorporating information from anchor B improves the estimator only when the estimates are sufficiently accurate, specifically when $\sigma_B^2 < (\beta+2)\,\sigma_A^2$. Otherwise, the localization accuracy decreases. The detailed derivation of the problem is provided in Appendix B. In scenarios where both anchors provide an equal number of estimates, the addition of the second anchor estimates enhances the localization accuracy only if

$$\sigma_B < \sqrt{3}\,\sigma_A\,. \tag{9}$$

These results are not limited to the sample-mean estimator, a similar conclusion is reached when using the LS estimator. In AoA-based localization, the covariance values σ_B^2 and σ_A^2 are differently influenced by the node position, as both anchors are in different physical positions. For instance, (34) illustrates how angles and distances from the node to the anchors define the GDOP, which is related to the RMSE and the Standard Deviation (SD). Therefore, the inequality in (9) can be a reasonable assumption only when the receivers are identical and much closer to each other than to the node. Even then, numerous situations may arise where (9) does not hold. In Fig. 2(a) and considering a direct analogy between SD and GDOP for simplicity, the error for a node displaced 2.2 m horizontally is already a factor $\sqrt{3}$ greater than that of a node located just below the anchor. This suggests that naive fusion

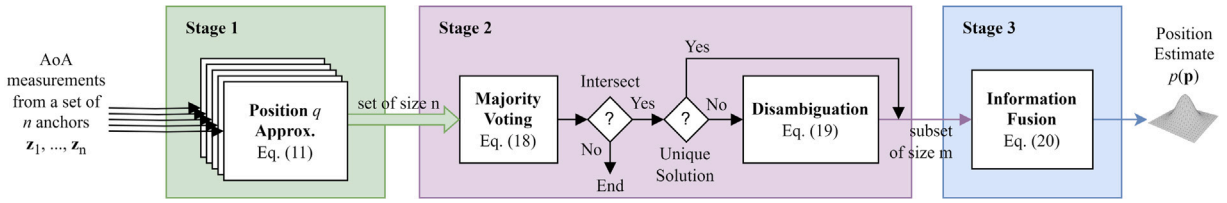

Fig. 4. Three-stage procedure outlining the proposed method for deriving the position estimate from a set of AoA measurements.

of estimates does not consistently enhance single-anchor performance for certain node positions, and these positions depend on the geometry of the anchor deployment.

To investigate this problem under more general conditions, we conducted Monte-Carlo simulations comparing the performance of a single-anchor solution against a two-anchor solution using the sample-mean estimator. Fig. 3 illustrates three comparisons in a standardized deployment setup and node positions, under simulated uncorrelated Additive White Gaussian Noise (AWGN). Metrics were computed from 10^6 estimates for each anchor and position point, assuming an SD of 10° for both azimuth and elevation angles.

In Fig. 3(a), the node of interest is positioned at $[8.5, 3, 0]^\mathsf{T}$ m (not shown). The red samples represent estimates of the node position from anchor B, with a 95th percentile error of 1.9 m. The blue samples are the averages of the independent estimates from anchors A and B, resulting in a greater 95th percentile error of 6.5 m due to the naive combination. Fig. 3(b) extends Fig. 3(a) to all points in the room, showing the RMSE of a single-anchor C solution minus the RMSE of a multi-anchor solution consisting of anchors A and B. Colder colors indicate where the single-anchor solution outperforms the naive combination in terms of RMSE. Fig. 3(c) depicts the CDF of position errors for multi-anchor A and B solution, with their separation varying from 1 to 9 m. The single-anchor C solution is presented as the baseline. The results highlight the nuanced conditions under which incorporating information from multiple anchors enhances or decreases the accuracy of position estimates in indoor localization.

In conclusion, the derived theoretical constraints emphasize the critical role of the deployment geometry in achieving improved localization. Mere fusion of estimates can jeopardize overall system accuracy due to the nonlinearity of the GDOP in the localization model. Consequently, careful consideration of anchor selection methods becomes imperative, particularly ones that consider the GDOP. In the context of indoor systems, the presence of multipath components in the received signal poses a substantial problem: These components introduce non-Gaussian errors that are also affected by the GDOP, thereby amplifying the necessity for advanced multi-anchor solutions with outlier rejection mechanisms.

5. Discrepancy filter for improved position estimation

This section presents the key contribution of the article: An efficient position estimation algorithm, referred to as the Discrepancy Filter (DF), designed to improve the precision of position estimates derived from a single signal emitted by a mobile node and received at distinct physical locations. The DF utilizes angular information provided by the available anchors. Notably, it addresses the challenges posed by realistic multipath channels by systematically discarding outlier information. It selectively chooses anchors whose information significantly improves accuracy, leading to a cost-effective solution suitable for affordable setups. Importantly, this algorithm can be computed in real-time on resource-constrained devices using only high-level angular or position measurements.

5.1. Solution overview

The DF is a spatial filter in the sense that it combines multiple observations of the same source obtained from different physical positions. It works by updating the probability regarding the location of the node with a selection of the information received from the anchors. More precisely, DF performs Bayesian inference with prior outlier discarding by approximating the posterior distribution $p(\mathbf{p}|\mathbf{z}_1, \dots, \mathbf{z}_m)$ given the observed angles in a subset of $1 < m \leq n$ selected anchors. Its operation can be summarized into three stages, illustrated in Fig. 4:

- S1 Approximating the position estimates distribution given the AoAs of each anchor (Section 5.2).
- S2 Rejecting outliers, that is, selecting a subset of the anchors using a majority voting scheme considering their approximations (Section 5.3).
- S3 Fusing the information from selected anchors through Bayesian Inference to derive the final position estimate (Section 5.4).

To define the final estimate, let us consider that each anchor independently estimates the position of the mobile node from the observed angles and let $p(\mathbf{p}|f(\mathbf{z}_1), \dots, f(\mathbf{z}_m)) = p(\mathbf{p}|\hat{\mathbf{p}}_{1:m})$ be the posterior we want to estimate, where we define $p(\mathbf{p}|\hat{\mathbf{p}}_{1:m}) \triangleq p(\mathbf{p}|\hat{\mathbf{p}}_1, \dots, \hat{\mathbf{p}}_m)$ for notation convenience. Recalling Bayes' theorem and assuming a Markov process with independent observations and anchors, the recursive expression of the unnormalized posterior is

$$p(\mathbf{p}|\hat{\mathbf{p}}_{1:m}) \propto p(\hat{\mathbf{p}}_m|\mathbf{p})\, p(\mathbf{p}|\hat{\mathbf{p}}_{1:m-1}), \tag{10}$$

which states that the posterior is proportional to the likelihood times the prior. Unfortunately, (10) is unavailable in closed form because of the nonlinear transformation in (3). Besides, the computation of (10) involves the integration over all dimensions of $\mathbf{p}$, which is expensive, or the use of Monte-Carlo sampling approximations that suffer from high variance and poor generalization when the number of samples is insufficient. Our proposal is to derive an approximation of the density that allows for a real-time implementation at the expense of introducing some bias.

5.2. Stage 1: Approximation of $p(\hat{\mathbf{p}}|\mathbf{p})$

To make (10) tractable in practice, we rely on conjugate distributions with the aim of computing the statistics of a random variable that undergoes a nonlinear transformation. In this subsection, the subscript i is omitted to avoid clutter. In addition, we will consider the height z_t to be known; the derivation of a 3D framework is left for future work because most IoT applications only require 2D localization.

Starting from an AoA observation $\mathbf{z}$, we first consider that:

- $\hat{\mathbf{p}}$ is obtained by solving for the point of intersection between the line formed by the anchor position $\mathbf{s}$ and direction $\mathbf{z}$ and the plane $z = z_t$ (or any similar method), yielding an estimate to the indoor feasible space with unknown uncertainty on the xy-plane.
- The variances of $\hat{\theta}$ and $\hat{\phi}$ are known and constant: given by others (e.g., derived from the FIM of the AoA estimation or from low-level measurements like the pseudo-spectrum of the AoA estimation algorithm [38]), experimentally pre-characterized with a set of controlled measurements or treated as hyperparameters to govern the outlier filter sensitivity in Stage 2.

Now let $q(\hat{\mathbf{p}}|\mathbf{p})$ be a tractable conditional distribution that approximates $p(\hat{\mathbf{p}}|\mathbf{p})$. Ideally, we would like to minimize a similarity metric between q and p to construct a bound on the likelihood, converting an intractable computation problem into a difficult optimization problem. To further reduce the computational burden, however, we derive an efficient solution based on a geometrically-derived unscented transformation.

Let us model the approximation using a multivariate Gaussian as

$$q(\hat{\mathbf{p}}|\mathbf{p}) = \mathcal{N}(\boldsymbol{\mu}|\mathbf{p}, \boldsymbol{\Sigma}|\mathbf{p}), \tag{11}$$

with moments $\boldsymbol{\mu}$ and $\boldsymbol{\Sigma}$. The justification for (11) is that (10) can be expressed in closed form while the multivariate expressiveness is able to retain good part of the shape of $p(\hat{\mathbf{p}}|\mathbf{p})$ in common indoor deployments. Indeed, due to the location geometry, the Gaussian-distributed azimuth and elevation angle errors propagate from the anchor position and form a conic-like section (a curve) upon intersection with the $z = z_t$ plane. The resulting section might be a hyperbola, a parabola or an ellipse depending on the distance from the node to the anchor.

To calculate the moments of q, we rely on a probabilistic interpretation of the geometric elliptical section: Its center defines the mean, and the lengths of the axes and their orientation define the covariance as a scaling and a rotation. Hereafter, we assume that the ellipse's major axis is defined by the elevation uncertainty and the minor axis by the azimuth uncertainty due to the typically higher error values in elevation angle estimation and its greater sensitivity to the node-anchor distance (see equations in Appendix A.1). If this assumption does not hold, the definitions can be interchanged. Besides, we omit the dependence of the moments on $\mathbf{p}$ for clarity.

The center $\boldsymbol{\mu}$ of the ellipse and the radius $a > 0$ of the major axis are defined by projecting the uncertainty of the elevation angle onto the positioning plane as

$$\boldsymbol{\mu} = \frac{1}{2}(\mathbf{p}^{\phi^+} + \mathbf{p}^{\phi^-}), \tag{12}$$

$$a = \|\mathbf{p}^{\phi^+} - \boldsymbol{\mu}\|_2, \tag{13}$$

where $\mathbf{p}^{\phi^+} = f(\mathbf{z} + [0, \sigma_\phi]^\mathsf{T})$ and $\mathbf{p}^{\phi^-} = f(\mathbf{z} - [0, \sigma_\phi]^\mathsf{T})$ are the plus and minus elevation angle SD error projections to the $z = z_t$ plane. Note that typically $\boldsymbol{\mu} \neq \hat{\mathbf{p}}$; instead, the center of the ellipse is shifted towards the furthest point because the error projections are not equidistant to $\hat{\mathbf{p}}$ (see the nonlinearity in Fig. 2). The radius $0 < b \leq a$ of the minor axis is similarly defined by projecting the uncertainty in the azimuth angle as

$$b = \frac{1}{2}\|\mathbf{p}^{\theta^+} - \mathbf{p}^{\theta^-}\|_2, \tag{14}$$

where $\mathbf{p}^{\theta^+} = f(f^{-1}(\boldsymbol{\mu}) + [\sigma_\theta, 0]^\mathsf{T})$ and $\mathbf{p}^{\theta^-} = f(f^{-1}(\boldsymbol{\mu}) - [\sigma_\theta, 0]^\mathsf{T})$ are the azimuth-type projections to the $z = z_t$ plane with any function $f^{-1} : \mathbb{R}^3 \mapsto \Omega^2$. Note that a and b can be close to 0 in good GDOP positions, e.g., below the anchor where AoA estimation may suffer depending on the hardware and algorithm used, so limiting both to a minimum value is beneficial in practice.

The ellipse's left-handed rotation α is defined by the angle between the vector formed by the anchor's position and the ellipse's center, $\mathbf{v}_e = \boldsymbol{\mu} - \mathbf{s}$, and the x-axis vector as:

$$\alpha = \operatorname{arctan2}(\mathbf{v}_x \times \mathbf{v}_e \cdot \mathbf{v}_n, \mathbf{v}_e \cdot \mathbf{v}_x), \tag{15}$$

where $\times$ and $\cdot$ respectively denote the cross and dot products, and $\mathbf{v}_x = [1, 0, 0]^\mathsf{T}$, $\mathbf{v}_n = [0, 0, 1]^\mathsf{T}$. Finally, we define the covariance matrix as a function of its eigenvectors and eigenvalues:

$$\boldsymbol{\Sigma} = \mathbf{R}\mathbf{S}\mathbf{S}\mathbf{R}^\mathsf{T}, \tag{16}$$

via a linear transformation using the product of the respective scaling and rotation matrices defined by

$$\mathbf{S} = \begin{bmatrix} a & 0 \\ 0 & b \end{bmatrix} \text{ and } \mathbf{R} = \begin{bmatrix} \cos\alpha & -\sin\alpha \\ \sin\alpha & \cos\alpha \end{bmatrix} \tag{17}$$

where a and b play the role of SDs.

5.3. Stage 2: Anchor selection (outlier rejection)

Similarly to communication systems where the channel determines the performance, in indoor localization accuracy is greatly affected by channel conditions. In particular, rather than AWGN, it is the presence of multipath components that limits the performance of the system. It is therefore advisable to incorporate a technique to discard atypical information caused by multipath or other adverse effects. To that end, we leverage the n computed approximations and apply a majority voting scheme to discard the outliers. The scheme is based on q, which adapts to the nonlinear GDOP because its moments are defined by an unscented transformation of the angles through the function f.

Let $N = \{1\,..\,n\}$ be the set of anchors and $E_i = \{\mathbf{x} \in \mathbb{R}^2 \mid (\mathbf{x}-\boldsymbol{\mu}_i)^\mathsf{T}\boldsymbol{\Sigma}_i^{-1}(\mathbf{x}-\boldsymbol{\mu}_i) \leq 1\}$, $i \in N$, their corresponding ellipses. We discard potential outliers in a majority voting scheme defined by the following problem

$$M^\star = \underset{M \subset N}{\arg\max}\, |M| \text{ s.t. } \bigcap_{i \in M} E_i \neq \emptyset\,. \tag{18}$$

When non-unique for $n > 3$, the resulting solution set $M^\star$ is disambiguated by comparison of the relative intersection areas:

$$M^* = \underset{M \in M^\star}{\arg\max} \frac{|\bigcap_{i \in M} E_i|}{|\bigcup_{i \in M} E_i|}\,. \tag{19}$$

The result is a subset of $m = |M^*|$ anchors $M^* \subset N$ without outliers.

The entire procedure is depicted in Fig. 4. Note that when none of the ellipses intersect then $M^\star$ contains all the subsets of one element in N. In this particular case we discard the information. No estimate of the position will be derived in the fusion stage: At least two different *intersecting* sources of information are needed, hence $1 < m \leq n$.

The pairwise intersection $E_i \cap E_j$ of two ellipses is first assessed roughly (e.g., by the distance between centers compared to the length of their axis or via bounding boxes) and only refined later if necessary (i.e., solving the corresponding 1D convex problem). It should be noted that other options exist for disambiguation instead of using (19), such as choosing the anchor with the minimum conic section, the two closest ellipses or trying again by increasing the size of the ellipses.

5.4. Stage 3: Information fusion

For a subset of m anchors, we iteratively update the prior distribution via the approximated likelihood starting from the prior $p(\mathbf{p}) \sim U$. Equivalently, we can initiate the process from any of the independent estimates. That is, for each anchor estimate, we consider the posterior distribution of the previous anchor as the prior for the current update step. Subsequently, the posterior distribution is defined as the unnormalized product of m Gaussian approximations as

$$\begin{aligned} p(\mathbf{p}|\hat{\mathbf{p}}_{1:m}) &\propto \prod_i^m p(\hat{\mathbf{p}}_i|\mathbf{p}) \\ &\approx \prod_i^m q(\hat{\mathbf{p}}_i|\mathbf{p}) \\ &\sim \prod_i^m \mathcal{N}\left(\boldsymbol{\mu}_i|\mathbf{p}, \boldsymbol{\Sigma}_i|\mathbf{p}\right) \\ &= \mathcal{N}\left(\tilde{\boldsymbol{\mu}}|\mathbf{p}, \tilde{\boldsymbol{\Sigma}}|\mathbf{p}\right), \end{aligned} \tag{20}$$

with moments defined by

$$\tilde{\boldsymbol{\Sigma}} = \left(\sum_i^m \boldsymbol{\Sigma}_i^{-1}\right)^{-1} \text{ and } \tilde{\boldsymbol{\mu}} = \tilde{\boldsymbol{\Sigma}}\left(\sum_i^m \boldsymbol{\Sigma}_i^{-1}\boldsymbol{\mu}_i\right). \tag{21}$$

Note that the fusion stage is technology-agnostic because its input is a set of position estimates, which may come from any localization solution. The only requirement in (20) is the use of conjugate distributions. Additionally, preliminary information may be incorporated into the initial prior, albeit its definition is not trivial [39]. For instance, the feasible space where the node is physically allowed to be is user-delimited in a localization system in consideration of the room topology. Therefore, Ω is different for each anchor measurement given that they are deployed in different positions. However, adding such information may not provide any benefit with respect to constraining the final estimate within a bounded space using geometric algebra.

6. Experimentation with Bluetooth Low Energy

This section evaluates the localization performance of the proposed filter and presents a performance comparison against well-known localization solutions. To evaluate our approach, we deployed a real-time test bed in an office building. We choose to experiment with BLE devices, as the direction finding capabilities of Bluetooth are highly adequate for indoor IoT localization needs. BLE is low cost, easy to implement and has low power consumption; consequently, it has a high return on investment for locating critical equipment or people in hospitals, warehouses, factories and supermarkets.

6.1. Deployment details

The localization system under evaluation was deployed in a common business office room with dimensions of $7.2 \times 8.5 \times 3$ m. The ceiling was made of metal plates, while the walls were plasterboard, except for one wall that was entirely covered by large windows. The room contained furniture, including chairs, tables, laptops and a locker. WiFi access points and other Bluetooth devices were observed transmitting in the 2.4 GHz band.

Three anchors were deployed at positions in meters $\mathbf{s}_1 = [3.7, 4.0, 2.8]^\intercal$', $\mathbf{s}_2 = [1.8, 6.9, 2.8]^\intercal$ and $\mathbf{s}_3 = [5.6, 6.9, 2.8]^\intercal$, forming a triangular shape at the top of the room (see Fig. 8). They divide the room into two distinct parts: The upper half encompasses measurement points located within the region defined by the anchors (referred to as the inner area), while the lower half includes points lying outside the convex hull of the anchors (referred to as the outer area). It is important to recall the impact of geometry on the GDOP, as illustrated in Fig. 2. In challenging geometric configurations like the outer area, the GDOP tends to be high, whereas in optimal geometric configurations like the inner area, the GDOP is low. Consequently, this deployment topology facilitates the simultaneous evaluation of the system's performance in both scenarios. We can then evaluate the algorithms in non-optimal conditions, demonstrating their robustness to anchor positions.

6.2. AoA hardware

The LAUNCHXL-CC26X2R1 development board from Texas Instruments (TI) was employed in BLE connectionless mode as the transmitting node for localization. This board was chosen due to its flexibility and well-documented features. The transmitting node was configured to transmit a packet every 100 ms, with an added CTE of 160 μs appended at the end.

On the other hand, the anchor utilized the TI's CC26X2R, an RF switch, and a custom 6-patch dual-polarized dipole antenna forming a uniform circular array. This antenna array underwent calibration in an anechoic chamber using a 1° angular resolution. The software employed for this setup was the RTLS Toolbox of the BLE5-Stack in TI's SDK v6.10. The anchors sampled the IQ components of the CTE from the received BLE signal at 1 MHz, with an 8-bit resolution, using 2 μs switching and sampling slots. This configuration adheres to the direction finding specification of Bluetooth 5.1 standard.

Notably, the methods investigated in this paper are AoA hardware-agnostic, eliminating the necessity for low-level measurements. This indicates that alternative hardware can be utilized for experimental purposes.

6.3. AoA estimation

Processing of the IQ samples obtained by the anchors was performed using the widely-used MUSIC algorithm, which initially addressed dual polarization, antenna switching, and compensated for the carrier frequency offset using the methods described in [40]. The output from the algorithm consisted of AoA estimates, without any quantification of uncertainty. These angle estimates were used for position estimation.

The accuracy of the angle estimates were analyzed in the given scenario to comprehend their variability and impact on achievable localization accuracy. For each anchor, we gathered 5×10^3 samples in total at ten calibrated positions over two distinct days. On the first day, for anchor at position $\mathbf{s}_1$, the average error was 3.2° for the azimuth angle and 4.7° for the elevation angle. Their respective SD were 8.1° and 11.1°. On the second day, the average azimuth and elevation angle errors were 1.3° and 5.9°, with SD of 2.3° and 8.2°, respectively. Higher error values were observed at anchors in positions $\mathbf{s}_2$ and $\mathbf{s}_3$. Generally, the error values fell within the anticipated performance range of current BLE indoor systems. The error distributions exhibited fat tails, signifying the day-to-day variability of errors and multipath effect that must be considered in the design of any evaluation procedure.

6.4. Evaluation description

To validate the proposed filter, we divided the room into a grid of 42 equispaced positions to serve as reference measurement points (see Fig. 8). The ground truth was derived through laser-ranging measurements obtained from a LIDAR at each reference position, meticulously aligned with the architectural map of the room. A total of 292,303 AoA measurements were obtained. 2400 packets were transmitted from each reference position and received simultaneously by each locator on two distinct days, under clear LOS conditions to ensure the acquisition of pertinent results. The utilized data are openly available on https://bitbucket.org/wineuoc/aoa-ble-dataset under experiment designations `2022_10_11_P42` and `2022_10_19_P42`.

To assess the performance of DF in comparison to other existing methods, we have evaluated its localization accuracy against the methods described in Table 1. To determine the node position, all algorithms employed consistent plain angle estimates obtained and processed during the measurement campaign. The resulting position estimates were constrained within the spatial boundaries

Table 1
List of alternative position estimation solutions evaluated and corresponding abbreviations.

Abbreviation	Description
A_i	The ith single-anchor 2D solution.
A_{rssi}	The single-anchor selection based on the highest RSSI value 2D solution. For example, Roshanaei et al. [41] and Cheng et al. [42] use RSSI in a k-nearest neighbors algorithm for anchor selection. Other *closeness* metrics have been omitted because of poor performance, such as elevation angle and the normalized magnitude between MUSIC pseudo-spectrums.
A_{best}	The selected best single-anchor estimates, post-processed using knowledge of actual measurement position. This process replicates the performance of an ideal anchor selection solution, wherein the most accurate estimate is chosen from a set of individual anchor estimates.
M_{avg}	The sample-mean estimate of the multiple anchors 2D independent solutions. For example, Monfared et al. [43] average the estimates by all anchors in their positioning step.
M_{LS}	The multi-anchor LS solution, that is, the minimization of the sum of perpendicular squared distances from the unique solution point to the lines given by the anchor positions and their received signal direction. For example, Watanabe [11] proposes a weighted LS solution and Koutris et al. [44] uses the LS algorithm with AoA estimates from a neural network.
M_{vMF}	A probabilistic approach based on modeling the angular uncertainty using a von Mises-Fisher (vMF) distribution. This approach is inspired by [20,22], where a similar BLE setup is used. We used the same objective function but our optimization routine is not the same. The AoAs in our objective were equally weighted. Our implementation used gradient ascent to solve the non-convex optimization problem. We initialized the algorithm using the average of the individual estimates from all anchors. The position was bounded to the room and no outlier rejection was performed. Convergence of the algorithm was assessed by monitoring the relative change of the objective. In comparison, [22] combines gradient ascent with an IRLS initialization routine, whereas [20] does not specify the optimization routine used.
M_{IAD}	A weighted LS solution incorporating an outlier rejection algorithm that relies on an identifying and discarding (IAD) strategy based on the LS cost function of the residuals. We implemented Algorithm 1 proposed by Xiong et al. [29] with a setting of $N = 2$, as our deployment consist of three anchors.

of the room for all the algorithms. The error metrics presented in this study are 2D and include the CDF, the RMSE and the CEP as represented by equations in (6). The entire codebase was implemented in Python and executed on an 11th Gen Intel i7-1185G7 processor.

In the practical implementation of DF, (18) was realized by examining the intersections of bounding boxes of ellipses using an R-Tree algorithm. The emphasis was placed on achieving scalability and real-time execution. The average runtime per position was 5 ms with a SD of 1 ms. To validate the approach, it was compared against an exact intersection-check implementation using image processing techniques, yielding identical results in the considered scenario. The pre-characterized variances $\hat{\theta}$ and $\hat{\phi}$ of anchor in position $\mathbf{s}_1$ were employed for anchors in positions $\mathbf{s}_1$, $\mathbf{s}_2$, and $\mathbf{s}_3$. The disambiguation stage given by (19) was not implemented due to the constraint $n = 3$. The evaluation of this stage in a larger deployment is deferred to future work.

6.5. Filter validation results

The primary objective of the initial evaluation was to validate DF as a multi-anchor locating solution. Additionally, it sought to appraise the proposed angle-error projection as a robust foundation for approximating position errors.

To quantify the influence of the projection size on both the anchor-selection stage and the overall performance of the system, we defined the ratio $R_\sigma \triangleq \sigma^{DF}_{\theta,\phi}/\hat{\sigma}_{\theta,\phi}$. The term $\hat{\sigma}_{\theta,\phi}$ was set to the largest value among the pre-characterized azimuth and elevation angle errors of the anchor in position $\mathbf{s}_1$. The term $\sigma^{DF}_{\theta,\phi}$ was employed to determine σ_ϕ of $\mathbf{p}^{\phi^+}$ in (12) and σ_θ of $\mathbf{p}^{\theta^+}$ in (14), ending up normalized to the physically calibrated value of $\hat{\sigma}_{\theta,\phi}$. This approach streamlined the analysis, enabling us to examine the sensitivity of DF to the single parameter R_σ that controls the uncertainty of the given AoAs before the unscented transformation of the error projection. Thus, it implicitly controls the size of the major and minor axis of the nonlinear projected ellipses and, in turn, the filter's tolerance for outliers. Note that $R_\sigma = 1$ directly considers the pre-characterized uncertainty of the AoAs, and equally weights the AoAs of each anchor; it is considered as the filter's default. Finally, we define the discard ratio R_d to account for the ratio of samples that the filter rejects.

The empirical CDF of the position errors, derived from 42 reference points utilizing the proposed DF method conditioned to R_σ, is illustrated in Fig. 5. Inclusion of the performance without considering the anchor selection stage (S2, Section 5.3) is incorporated to underscore its significance. The gray dotted line indicates a decline in accuracy when S2 is omitted, representing the naive scenario with no samples filtered out ($R_d = 0$).

Concerning the role of R_σ, low values theoretically result in smaller projected ellipses, thereby reducing the filter's tolerance to outlier samples. Simultaneously, an increase in localization accuracy is anticipated if the most accurate AoA estimates are transmitted to the information fusion stage. Fig. 5 empirically validates this anticipated behavior. For instance, when $R_\sigma = 0.4$, the probability of the error being less than or equal to 1 m is 0.86, albeit at the cost of discarding 52% of the received information. Conversely, $\mathbb{P}(\epsilon \leq 1 \mid R_\sigma = 2) = 0.69$ is achieved with a discard ratio of $R_d = 0.1$.

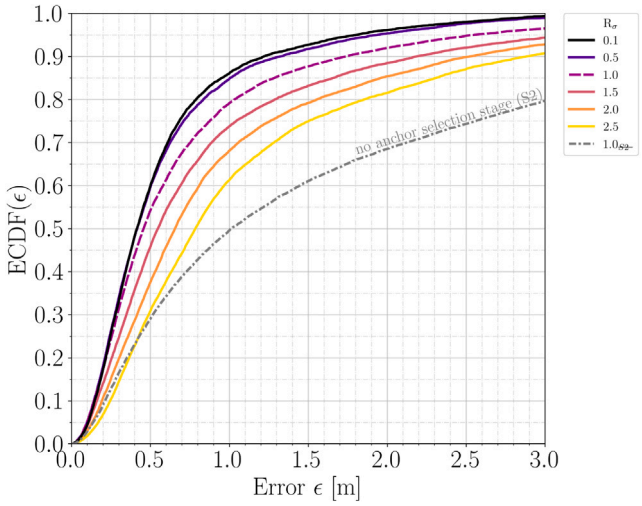

Fig. 5. The empirical CDF of the errors obtained using the proposed DF conditioned to different R_σ.

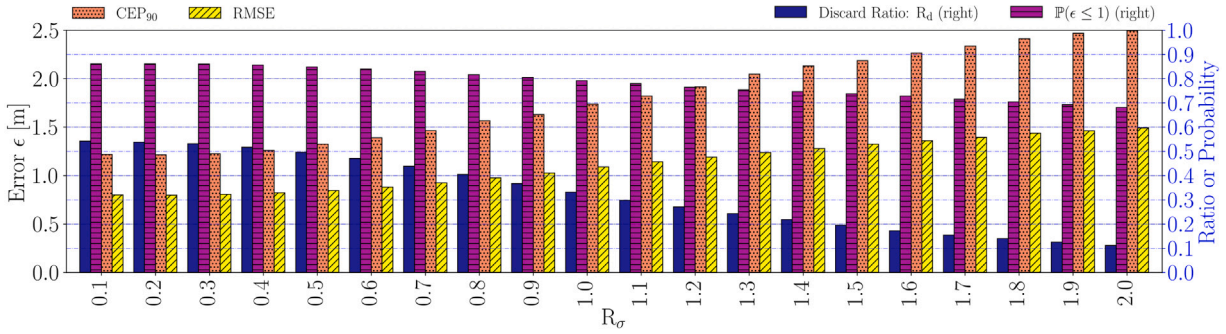

Fig. 6. DF performance sensitivity to R_σ, which roughly controls how tolerant is the filter to outlier measurements.

Interestingly, the observed error distributions exhibit fat tails, meaning larger position error values persist even after filtering out outliers. It is noteworthy that for this phenomenon to occur, two or three anchors must generate sufficiently different errors in their AoA estimates, leading to intersections of ellipses projected onto the xy-plane that are not discarded. This implies that anchor information obtained at distinct spatial positions results in similar and incorrect position estimates, suggesting the presence of correlated spatial errors in the AoA estimates that the DF method does not overcome.

In addition, Fig. 6 shows in detail how the discard ratio relates to common error metrics. The filter's performance sensitivity to R_σ is shown for values in the range $[0.1, 2]$ at 0.1 increments. As R_σ decreases, the filter becomes less tolerant to outliers, thus more samples are discarded. This translates into a decrease in the RMSE and CEP_{90} metrics. It is worth mentioning that the tradeoff is not linear; increasing R_σ from 0.6 to 0.8 lowers the discard ratio, but going from 1.6 to 1.8 does not lower it the same amount.

The conclusion therefore is that the filter is able to leverage the spatial information received to increase accuracy, validating the approximation, selection and fusion stages. It offers the possibility to treat R_σ as a hyperparameter, which may come in handy for some use cases where a high discard ratio may cause issues. The R_d value bounded to the expected number of packets to be received by the anchor can be used as a control variable of a Proportional–Integral–Derivative (PID) controller. The PID could be designed to increase or decrease R_σ to match the desired output rate of the filter, thus adapting to signal propagation conditions.

6.6. Performance comparison results

The second evaluation was conducted to assess the effectiveness of DF in comparison to the methods outlined in Table 1. The objective was to quantitatively analyze and comprehend the advantages of employing DF in multi-anchor deployments.

Utilizing multiple anchors is imperative due to the inadequacies of single-anchor implementations in achieving the desired accuracy across various localization-area sizes encountered in common use cases. The enhancements in performance should not only arise from the inner area formed by the anchor but also, significantly, from the outer area. This is crucial to ensure that the cost-benefit ratio of the localization solution is increased, rendering it more appealing.

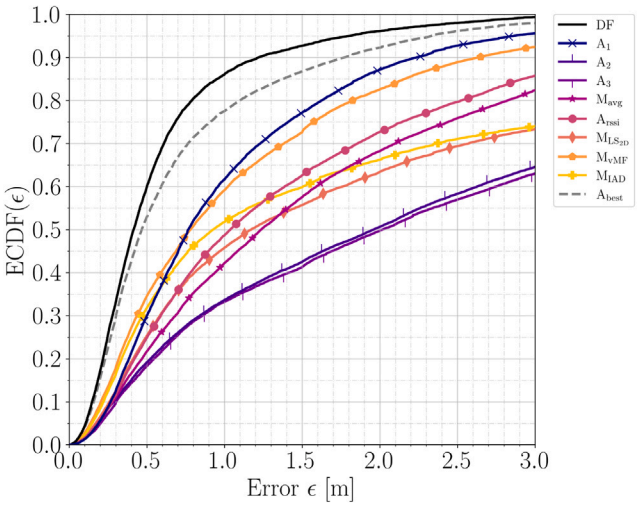

Fig. 7. The performance of the best proposed DF ($R_\sigma = 0.2$) compared against the other localization solutions.

The individual localization performance of each anchor is illustrated in Fig. 7, providing insight into the challenges faced by multi-anchor approaches. Anchors A_2 and A_3 exhibit notably lower performance in comparison to A_1 at position $\mathbf{s}_1$, primarily due to the impact of GDOP in the deployment topology. The majority of measurement points for A_2 and A3 are situated farther away, although all points are considered in the CDF. The ideal single-anchor selection, denoted as A_{best} and processed a posteriori among the three anchors, is also presented to serve as a benchmark for single-anchor selection performance.

Fig. 7 clearly demonstrates that DF outperforms all evaluated methods and is the sole approach enhancing the single-anchor localization of A_1. Moreover, DF surpasses the performance of A_{best}, indicating that fusing estimates of the filter (S3, Section 5.4) enhances accuracy. Naive multi-anchor solutions, such as M_{avg} and M_{LS}, generally fail to effectively leverage information from all three anchors. The RSSI-based anchor selection method, A_{rssi}, also exhibits subpar overall performance. M_{vMF} outperforms the naive multi-anchor solutions and A_{rssi}, underscoring the added value of probabilistic approaches based on directional statistics. It is worth noting that improved performance can be anticipated by attenuating the impact of outliers in the initialization, as discussed in [22]. For example, applying an outlier rejection strategy to the LS estimator such as M_{IAD} led to improved results with respect to M_{LS}.

While the CDF retains the majority of statistical information when compared to single-value metrics, it lacks spatial information, making it challenging to gain insights into the solution's behavior across different positions in space. To address this limitation, Fig. 8 illustrates spatial heatmaps, visually presenting the median value (CEP_{50}) of errors in each area of the room. In practice, the spatial performance of A_1, A_2, and A_3 (refer to Figs. 8(a), 8(b), 8(c), respectively) aligns with the predictions of GDOP, except for a slight decrease in accuracy just below the anchor. The impact of GDOP nonlinearity for far distances as detailed in Section 4.1 is evident in the figures for A_2 and A_3.

Concerning anchor selection, A_{rssi} (Fig. 8(g)) enhances accuracy for positions very close to anchors, but performance diminishes for positions further away due to the poor correlation between RSSI and node-to-anchor distance in a multipath-rich BLE environment. M_{avg} (Fig. 8(e)) improves accuracy in the inner area but decreases it in the outer area. Similar trends were observed for M_{LS}, leading to their omission. These results align with the findings in Section 4.2, emphasizing that increasing the number of anchors in naive multi-anchor methods does not universally enhance performance in all positions. The method M_{IAD} surpasses naive approaches by effectively rejecting outliers. Nevertheless, its accuracy diminishes significantly at considerable distances beyond the outer area, making it unable to provide precise estimates.

In contrast, the DF (Fig. 8(h)) significantly improves accuracy in both inner and outer areas compared to multi-anchor approaches, validating DF as a practical and cost-effective localization solution. DF is likely to require a lower anchor density to achieve a specific level of accuracy due to its effective performance beyond the convex hull of the anchors. Compared to A_1, DF consistently improves localization in most measured points, except for the farthest points in the lower part of the room, where accuracy is nearly equivalent to A_1. It is crucial to note that the DF necessitates at least two different sources of information to derive an estimate, showcasing its capability to leverage received information accurately.

7. Conclusion

This paper has delved into the nonlinear problem associated with indoor position estimation through AoA measurements and proposed a filtering technique designed to address it effectively. By assimilating data from diverse spatial sources, our approach involves the identification and elimination of anomalous data. The subsequent combination of information through Bayesian inference enhances the accuracy of indoor localization. The validation of our method as a multi-anchor solution for IoT-based

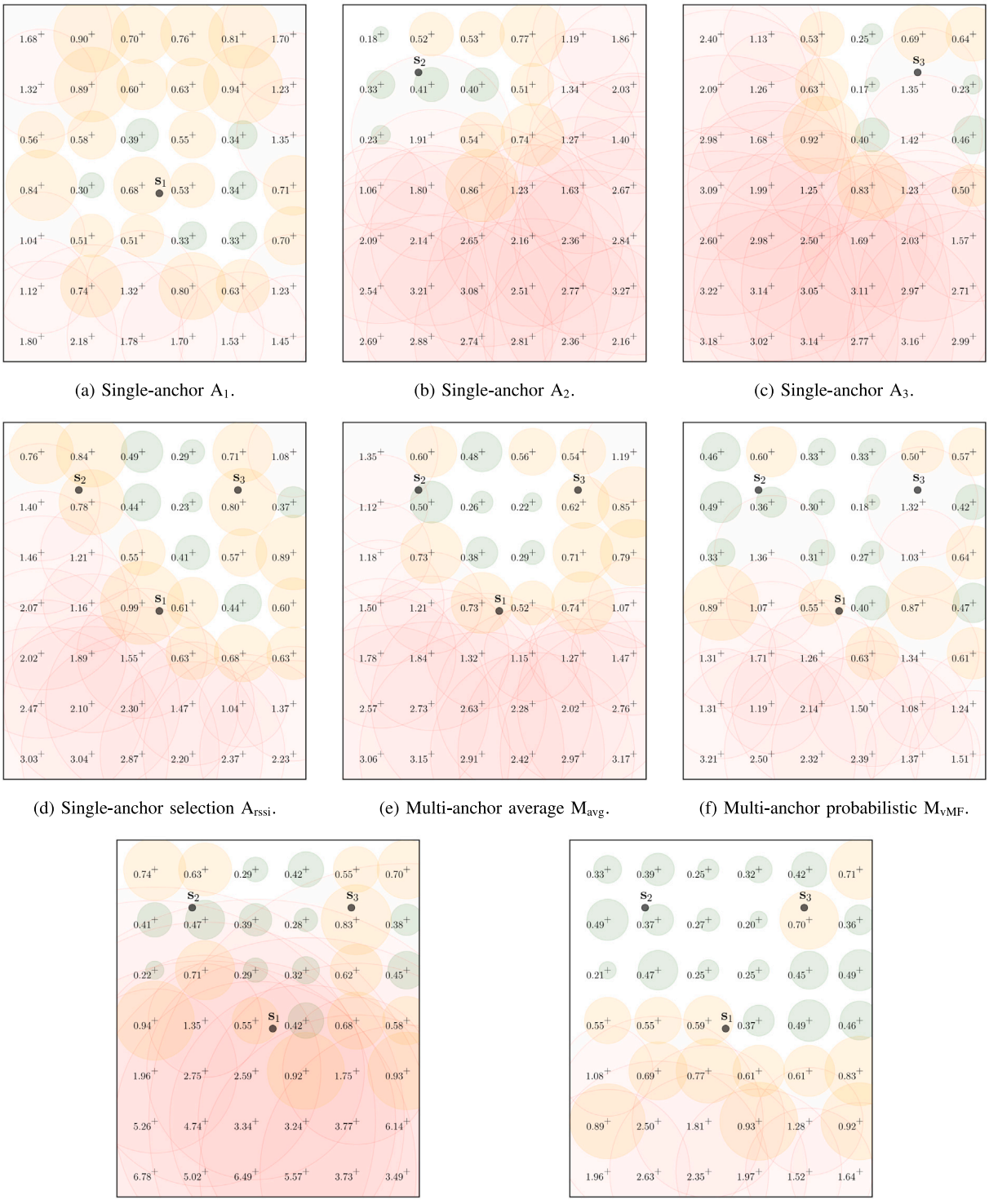

(a) Single-anchor A_1. (b) Single-anchor A_2. (c) Single-anchor A_3.

(d) Single-anchor selection A_{rssi}. (e) Multi-anchor average M_{avg}. (f) Multi-anchor probabilistic M_{vMF}.

(g) Multi-anchor LS + IAD M_{IAD}. (h) Proposed DF ($R_\sigma = 1$).

Fig. 8. Spatial performance of the localization solutions. Black circles depict the anchors involved. Cross markers depict the measurement points, and text labels explicitly show the median value of the errors. The radius of the circles is defined by the median of the errors. Color is green, orange or red when the median value is in $[0, 0.5]$, $(0.5, 1]$ or $(1, \infty)$ m, respectively.

indoor localization underscores its robustness in filtering out outlier measurements originating from temporary channel impairments or poorly positioned nodes in terms of geometric dilution of precision. Importantly, the cost-benefit ratio associated with the incorporation of additional information, whether in the form of angular measurements or position estimates, provides a distinct advantage over alternative approaches.

It is noteworthy that introducing information into the proposed filter does not compromise accuracy unless the errors derived from it exhibit spatial correlation. Therefore, the inclusion of additional information is likely to enhance overall performance. This could entail sourcing supplementary information from diverse location technologies within the heterogeneous IoT framework or incorporating secondary angle estimates resulting from multipath components in the signal direction-finding algorithm, provided low-level measurements are accessible. Our proposed filtering method thus emerges as a promising solution with practical implications for improving the reliability and precision of indoor positioning systems.

Immediate future work will aim to adapt our method to use directional statistics, which make use of a more natural support for the angular measurements but currently derives into an expensive optimization process. We will undertake an evaluation to assess the trade-off associated with utilizing directional statistics to model angular uncertainty, especially within the context of larger deployments in the IoT.

CRediT authorship contribution statement

Guillem Boquet: Writing – review & editing, Writing – original draft, Visualization, Software, Methodology, Investigation, Formal analysis, Data curation, Conceptualization. **Aleix Boquet-Pujadas:** Writing – review & editing, Formal analysis, Conceptualization. **Ivan Pisa:** Validation, Resources. **Anand Dabak:** Validation, Supervision, Resources. **Xavier Vilajosana:** Writing – review & editing, Conceptualization, Supervision, Resources, Project administration, Methodology, Investigation, Funding acquisition. **Borja Martinez:** Writing – review & editing, Conceptualization, Validation, Supervision, Resources, Project administration, Methodology, Investigation, Funding acquisition.

Declaration of competing interest

The authors declare that they have no known competing financial interests or personal relationships that could have appeared to influence the work reported in this paper.

Data availability

Data link is found in the paper.

Appendix A. Derivation of the geometric dilution of precision

The Cramér-Rao inequality provides a lower bound for the covariance of any unbiased estimator [35]. In particular, for an unbiased estimator $\hat{\mathbf{p}}$ of $\mathbf{p}$, the CBR reads

$$\mathbf{P} \geq \mathbf{M}^{-1} \triangleq \mathrm{CRB}\,. \tag{22}$$

Here $\mathbf{M}$ is the FIM, which quantifies the amount of information that the observations $\mathcal{Z}_n$ carry about the unobservable $\mathbf{p}$. Note that maximizing the information minimizes the covariance of the error. The FIM is defined by

$$\mathbf{M} = \mathbb{E}_{\mathbf{p}}\left[\left[\nabla_{\mathbf{p}} \ln p\left(\mathcal{Z}_n|\mathbf{p}\right)\right]\left[\nabla_{\mathbf{p}} \ln p\left(\mathcal{Z}_n|\mathbf{p}\right)\right]^{\mathsf{T}}\right]. \tag{23}$$

Consider now that all anchor noise is independent of the position of the mobile node. We model them as i.i.d. zero-mean Gaussian variables: $\mathbf{w}_i \sim \mathcal{N}\left(\mathbf{0}, \mathbf{W}_i\right)$, where

$$\mathbf{W}_i = \begin{bmatrix} \sigma_{\theta_i}^2 & 0 \\ 0 & \sigma_{\phi_i}^2 \end{bmatrix} \tag{24}$$

is the covariance matrix and σ_{θ_i}, and σ_{ϕ_i} are the SD of the observed azimuth and elevation angles at the ith anchor. The likelihood function of p given the independent Gaussian observations $\mathcal{Z}_n$ is

$$\begin{aligned} p(\mathcal{Z}_n|\mathbf{p}) = \prod_{i=1}^{n} & \frac{1}{2\pi \det(\mathbf{W}_i)^{1/2}} \\ & \exp\left(-\frac{1}{2}(\mathbf{z}_i - \mathbf{h}_i(\mathbf{p}))^{\mathsf{T}}\mathbf{W}_i^{-1}(\mathbf{z}_i - \mathbf{h}_i(\mathbf{p}))\right). \end{aligned} \tag{25}$$

Under these assumptions – and when the error covariance is independent of $\mathbf{p}$ – the FIM can be written as a summation over the contribution of each anchor [45]:

$$\mathbf{M} = \sum_{i=1}^{n} \mathbf{J}_i^{\mathsf{T}}\mathbf{W}_i^{-1}\mathbf{J}_i\,, \tag{26}$$

where $\mathbf{J}_i$ is the Jacobian of the observation vector at the ith anchor with respect to $\mathbf{p}$,

$$\mathbf{J}_i \triangleq \nabla_{\mathbf{p}} \mathbf{h}_i^{\top}(\mathbf{p}) = \begin{bmatrix} \frac{\partial h_i^{\theta}(\mathbf{p})}{\partial x_t} & \frac{\partial h_i^{\phi}(\mathbf{p})}{\partial x_t} \\ \frac{\partial h_i^{\theta}(\mathbf{p})}{\partial y_t} & \frac{\partial h_i^{\phi}(\mathbf{p})}{\partial y_t} \\ \frac{\partial h_i^{\theta}(\mathbf{p})}{\partial z_t} & \frac{\partial h_i^{\phi}(\mathbf{p})}{\partial z_t} \end{bmatrix}. \tag{27}$$

The trace of the CRB is the minimum possible localization mean squared error for the unbiased estimator [45]. This criterion assumes that the localization algorithm in use is almost efficient, so that its error covariance can be approximated by the CRB. A variant of the trace measure is the GDOP defined as

$$\mathrm{GDOP} = \sqrt{\mathrm{Tr}\left(\mathbf{M}^{-1}\right)}\,|_{\mathbf{W}=\mathbf{I}}\ . \tag{28}$$

It is commonly used to assess GNSS [46]. Note that the expression in (28) only reflects the geometric effect on the RMSE when $\mathbf{W} = \mathbf{I}$, where $\mathbf{I}$ denotes the identity matrix [47]. Also, it is used for evaluating system designs, analogously to what Shannon's capacity represents in communication systems. Some optimal anchor placement strategies aim to minimize the trace of the inverse FIM [45,48].

A.1. Jacobian expression for single-anchor localization based on AoA measurements

Considering the AoA observation model in (3), the elements of the Jacobian (27) needed to calculate the GDOP are:

$$\mathrm{J}_{1,1}^{(i)} = -\frac{y_t - y_i}{(x_t - x_i)^2 + (y_t - y_i)^2} \tag{29}$$

$$\mathrm{J}_{2,1}^{(i)} = \frac{x_t - x_i}{(x_t - x_i)^2 + (y_t - y_i)^2} \tag{30}$$

$$\mathrm{J}_{3,1}^{(i)} = 0 \tag{31}$$

$$\mathrm{J}_{1,2}^{(i)} = -\frac{(x_t - x_i)(z_t - z_i)}{d_i^3 \sqrt{1 - \left(\frac{z_t - z_i}{d_i}\right)^2}} \tag{32}$$

$$\mathrm{J}_{2,2}^{(i)} = -\frac{(y_t - y_i)(z_t - z_i)}{d_i^3 \sqrt{1 - \left(\frac{z_t - z_i}{d_i}\right)^2}} \tag{33}$$

$$\mathrm{J}_{3,2}^{(i)} = \frac{1}{d_i} \sqrt{1 - \left(\frac{z_t - z_i}{d_i}\right)^2}\,. \tag{34}$$

In the case where z_t is known in advance, we instead get $\mathrm{J}_{3,1}^{(i)} = \mathrm{J}_{3,2}^{(i)} = 0$.

Appendix B. Impact of multi-anchor independent estimates on the sample-mean position estimator

Let $\{\hat{\mathbf{p}}_1, \ldots, \hat{\mathbf{p}}_K\}$ be the set of K i.i.d. estimates obtained from anchor A. The *kth* sample is modeled by

$$\hat{\mathbf{p}}_k = \mathbf{p} + \mathbf{v}_k, \tag{35}$$

where $\mathbf{v}_k \sim \mathcal{N}\left(\mathbf{0}, \sigma_A^2\,\mathbf{I}\right)$ accounts for the error in the coordinates measured from anchor A with a covariance of $\mathrm{Cov}(\mathbf{v}_k) = \sigma_A^2\,\mathbf{I}$. This is the most favorable noise case of AWGN. The sample-mean estimator is expressed as

$$\hat{\mathbf{p}}_A = \frac{1}{K} \sum_{k=1}^{K} \hat{\mathbf{p}}_k\,. \tag{36}$$

The error of this estimator is then normally distributed with zero mean and finite covariance $\mathrm{Cov}(\hat{\mathbf{p}}_A) = \mathrm{Cov}(\hat{\mathbf{p}}_k)/K$:

$$\hat{\mathbf{p}}_A - \mathbf{p} \sim \mathcal{N}\left(\mathbf{0}, \frac{\sigma_A^2}{K}\,\mathbf{I}\right). \tag{37}$$

Now let $\{\hat{\mathbf{q}}_1, \ldots, \hat{\mathbf{q}}_L\}$ be the set of L i.i.d. estimates obtained from a second anchor B. Each sample is modeled analogously to (35) but with covariance $\sigma_B^2\,\mathbf{I}$. If one incorporates the new information provided by B, the estimator of the position becomes

$$\hat{\mathbf{p}}_{AB} = \frac{1}{K + L} \left(\sum_{k=1}^{K} \hat{\mathbf{p}}_k + \sum_{l=1}^{L} \hat{\mathbf{q}}_l \right). \tag{38}$$

Assuming $\hat{\mathbf{p}}_k$ and $\hat{\mathbf{q}}_l$ are independent, the new covariance reads

$$\mathrm{Cov}(\hat{\mathbf{p}}_{AB}) = \frac{K\,\sigma_A^2 + L\,\sigma_B^2}{(K + L)^2}\,\mathbf{I}. \tag{39}$$

The error of the combined estimator is therefore

$$\hat{\mathbf{p}}_{AB} - \mathbf{p} \sim \mathcal{N}\left(\mathbf{0}, \frac{\sigma_A^2}{K}\frac{1+\beta\gamma^2}{(1+\beta)^2}\mathbf{I}\right), \tag{40}$$

where $\beta = L/K$ and $\gamma = \sigma_B/\sigma_A$ highlight the scaling factor introduced in the covariance. Note that (37) is the limit of (40) as L tends to zero. The scaling in (40) reflects how the accuracy of the estimator is affected by the inclusion of the estimates provided by the second anchor B. This result should be treated as a lower bound because only AWGN is considered in the derivation.

References

[1] T.-M. Choi, S. Kumar, X. Yue, H.-L. Chan, Disruptive technologies and operations management in the industry 4.0 era and beyond, Prod. Oper. Manage. 31 (1) (2022) 9–31.
[2] P.S. Farahsari, A. Farahzadi, J. Rezazadeh, A. Bagheri, A survey on indoor positioning systems for iot-based applications, IEEE Internet Things J. 9 (10) (2022) 7680–7699.
[3] F. Zafari, A. Gkelias, K.K. Leung, A survey of indoor localization systems and technologies, IEEE Commun. Surv. Tutor. 21 (3) (2019) 2568–2599.
[4] H. Kopetz, W. Steiner, Internet of things, in: Real-time systems: design principles for distributed embedded applications, Springer, 2022, pp. 325–341.
[5] M. Woolley, Bluetooth Core Specification Version 5.1 Feature Overview, Bluetooth Technol. Web. (2021) (Accessed 28 February 2023).
[6] M. Woolley, Bluetooth SIG, Bluetooth direction finding: A technical overview, Bluetooth Technol. Web. (2021) (Accessed 28 February 2023).
[7] G. Pau, F. Arena, Y.E. Gebremariam, I. You, Bluetooth 5.1: An analysis of direction finding capability for high-precision location services, Sensors 21 (11) (2021) 3589.
[8] R. Peng, M.L. Sichitiu, Angle of arrival localization for wireless sensor networks, in: 2006 3rd Annual IEEE Communications Society on Sensor and Ad Hoc Communications and Networks, Vol. 1, IEEE, 2006, pp. 374–382.
[9] X. Guo, N. Ansari, F. Hu, Y. Shao, N.R. Elikplim, L. Li, A survey on fusion-based indoor positioning, IEEE Commun. Surv. Tutor. 22 (1) (2019) 566–594.
[10] H. Krim, M. Viberg, Two decades of array signal processing research: the parametric approach, IEEE Signal Process. Mag. 13 (4) (1996) 67–94.
[11] F. Watanabe, Wireless sensor network localization using AoA measurements with two-step error variance-weighted least squares, IEEE Access 9 (2021) 10820–10828.
[12] A.G. Lingren, K.F. Gong, Position and velocity estimation via bearing observations, IEEE Trans. Aerosp. Electron. Syst. (4) (1978) 564–577.
[13] M. Gavish, A.J. Weiss, Performance analysis of bearing-only target location algorithms, IEEE Trans. Aerosp. Electron. Syst. 28 (3) (1992) 817–828.
[14] K. Doğançay, Bearings-only target localization using total least squares, Signal Process. 85 (9) (2005) 1695–1710.
[15] Y. Zheng, M. Sheng, J. Liu, J. Li, Exploiting AoA estimation accuracy for indoor localization: A weighted AoA-based approach, IEEE Wireless Commun. Lett. 8 (1) (2018) 65–68.
[16] M. Naseri, H. Amiri, A novel bearing-only localization for generalized Gaussian noise, Signal Process. 189 (2021) 108248.
[17] D. Munoz, F.B. Lara, C. Vargas, R. Enriquez-Caldera, Position Location Techniques and Applications, Academic Press, 2009.
[18] D.R. Philips, E. Salami, H. Ramiah, J. Kanesan, Location accuracy optimization in Bluetooth Low Energy (BLE) 5.1 based indoor positioning system (IPS)-a machine learning approach, IEEE Access (2023).
[19] W. Ding, S. Chang, J. Li, A novel weighted localization method in wireless sensor networks based on hybrid RSS/AoA measurements, IEEE Access 9 (2021) 150677–150685.
[20] C. Geng, T.E. Abrudan, V.-M. Kolmonen, H. Huang, Experimental study on probabilistic ToA and AoA joint localization in real indoor environments, in: ICC 2021-IEEE International Conference on Communications, IEEE, 2021, pp. 1–6.
[21] H. Nurminen, L. Suomalainen, S. Ali-Loytty, R. Piché, 3D angle-of-arrival positioning using von mises-Fisher distribution, in: 2018 21st International Conference on Information Fusion, FUSION, IEEE, 2018, pp. 2036–2041.
[22] M. Henninger, T.E. Abrudan, S. Mandelli, M. Arnold, S. Saur, V.-M. Kolmonen, S. Klein, T. Schlitter, S.T. Brink, Probabilistic 5G indoor positioning proof of concept with outlier rejection, in: 2022 Joint European Conference on Networks and Communications & 6G Summit, 2022, pp. 249–254.
[23] Q. Yan, J. Chen, G. Ottoy, L. De Strycker, Robust AOA based acoustic source localization method with unreliable measurements, Signal Process. 152 (2018) 13–21.
[24] N.H. Nguyen, K. Doğançay, E.E. Kuruoğlu, An iteratively reweighted instrumental-variable estimator for robust 3-D AOA localization in impulsive noise, IEEE Trans. Signal Process. 67 (18) (2019) 4795–4808.
[25] G. Zanca, F. Zorzi, A. Zanella, M. Zorzi, Experimental comparison of RSSI-based localization algorithms for indoor wireless sensor networks, in: Proceedings of the Workshop on Real-World Wireless Sensor Networks, 2008, pp. 1–5.
[26] T. Van der Vorst, T.-H. Nguyen, S. Monfared, A. Benlarbi-Delai, J. Sarrazin, F. Horlin, P. De Doncker, Anchor selection in angle-of-arrival estimation-based localization using polynomial chaos expansions, in: 2020 IEEE 91st Vehicular Technology Conference, VTC2020-Spring, IEEE, 2020, pp. 1–5.
[27] S. Monfared, E.I.P. Copa, P. De Doncker, F. Horlin, AoA-based iterative positioning of IoT sensors with anchor selection in NLOS environments, IEEE Trans. Veh. Technol. 70 (6) (2021) 6211–6216.
[28] Q. Yan, J. Chen, J. Zhang, W. Zhang, Robust AOA-based source localization using outlier sparsity regularization, Digit. Signal Process. 112 (2021) 103006.
[29] W. Xiong, J. Bordoy, A. Gabbrielli, G. Fischer, D.J. Schott, F. Höflinger, J. Wendeberg, C. Schindelhauer, S.J. Rupitsch, Two efficient and easy-to-use NLOS mitigation solutions to indoor 3-D AOA-based localization, in: 2021 International Conference on Indoor Positioning and Indoor Navigation, IPIN, IEEE, 2021, pp. 1–8.
[30] A. Toloei, S. Niazi, State estimation for target tracking problems with nonlinear Kalman filter algorithms, Int. J. Comput. Appl. 98 (17) (2014).
[31] M.V. Gamarra, S. Papaharalabos, F. Rezaei, D. Bartlett, P. Karlsson, Seamless indoor and outdoor positioning with hybrid bluetooth AoA and GNSS signals, in: 2023 13th International Conference on Indoor Positioning and Indoor Navigation, IPIN, IEEE, 2023, pp. 1–6.
[32] L. Schmitt, W. Fichter, Continuous singularity free approach to the three-dimensional bearings-only tracking problem, J. Guid. Control Dyn. 39 (12) (2016) 2673–2682.
[33] E. Naftali, N.C. Makris, Necessary conditions for a maximum likelihood estimate to become asymptotically unbiased and attain the cramer–rao lower bound. Part I. General approach with an application to time-delay and Doppler shift estimation, J. Acoust. Soc. Am. 110 (4) (2001) 1917–1930.
[34] D.J. Torrieri, Statistical theory of passive location systems, IEEE Trans. Aerosp. Electron. Syst. (2) (1984) 183–198.
[35] S.M. Kay, Fundamentals of Statistical Signal Processing: Estimation Theory, Prentice-Hall, Inc., 1993.
[36] Q. Zhu, K. Niu, C. Dong, Y. Wang, A novel angle of arrival (AOA) positioning algorithm aided by location reliability prior information, in: 2021 IEEE Wireless Communications and Networking Conference, WCNC, IEEE, 2021, pp. 1–6.
[37] L. Rui, K. Ho, Bias analysis of maximum likelihood target location estimator, IEEE Trans. Aerosp. Electron. Syst. 50 (4) (2014) 2679–2693.
[38] N. BniLam, G. Ergeerts, D. Subotic, J. Steckel, M. Weyn, Adaptive probabilistic model using angle of arrival estimation for IoT indoor localization, in: 2017 International Conference on Indoor Positioning and Indoor Navigation, IPIN, IEEE, 2017, pp. 1–7.
[39] A.R. Syversveen, Noninformative Bayesian priors. Interpretation and problems with construction and applications, Preprint Statist. 3 (3) (1998) 1–11.

[40] S. Cloudt, Bluetooth Low Energy Direction Finding on Embedded Hardware by Mitigating Carrier Frequency Offset and Multipath Fading (Ph.D. thesis), Eindhoven University of Technology Eindhoven, The Netherlands, 2021.
[41] M. Roshanaei, M. Maleki, Dynamic-KNN: A novel locating method in WLAN based on angle of arrival, in: 2009 IEEE Symposium on Industrial Electronics & Applications, Vol. 2, IEEE, 2009, pp. 722–726.
[42] C. Cheng, J. Guan, C. Wang, P. Wang, F. Shi, An improved indoor positioning method based on received signal strengths, in: 2022 14th International Conference on Measuring Technology and Mechatronics Automation, ICMTMA, IEEE, 2022, pp. 317–321.
[43] S. Monfared, T.-H. Nguyen, T. Van der Vorst, P. De Doncker, F. Horlin, Iterative NDA positioning using angle-of-arrival measurements for IoT sensor networks, IEEE Trans. Veh. Technol. 69 (10) (2020) 11369–11382.
[44] A. Koutris, T. Siozos, Y. Kopsinis, A. Pikrakis, T. Merk, M. Mahlig, S. Papaharalabos, P. Karlsson, Deep learning-based indoor localization using multi-view BLE signal, Sensors 22 (7) (2022) 2759.
[45] S. Xu, K. Doğançay, Optimal sensor placement for 3-D angle-of-arrival target localization, IEEE Trans. Aerosp. Electron. Syst. 53 (3) (2017) 1196–1211.
[46] I. Sharp, K. Yu, Y.J. Guo, GDOP analysis for positioning system design, IEEE Trans. Veh. Technol. 58 (7) (2009) 3371–3382.
[47] C. Yang, L. Kaplan, E. Blasch, Performance measures of covariance and information matrices in resource management for target state estimation, IEEE Trans. Aerosp. Electron. Syst. 48 (3) (2012) 2594–2613.
[48] K. Doğançay, H. Hmam, Optimal angular sensor separation for AOA localization, Signal Process. 88 (5) (2008) 1248–1260.